HYDROLOGICAL PROCESSES
Hydrol. Process. **19**, 2755–2774 (2005)
Published online 19 April 2005 in Wiley InterScience (www.interscience.wiley.com). DOI: 10.1002/hyp.5784

An approach to using snow areal depletion curves inferred from MODIS and its application to land surface modelling in Alaska

Stephen J. Déry,[1]* Vincent V. Salomonson,[2] Marc Stieglitz,[3] Dorothy K. Hall[4] and Igor Appel[5]

[1] *Lamont–Doherty Earth Observatory, Columbia University, Palisades, NY, USA*
[2] *Earth Sciences Directorate, NASA GSFC, Greenbelt, MD, USA*
[3] *School of Civil and Environmental Engineering and School of Earth and Atmospheric Sciences, Georgia Institute of Technology, Atlanta, GA, USA*
[4] *Hydrological Sciences Branch, NASA GSFC, Greenbelt, MD, USA*
[5] *Raytheon ITSS, Upper Marlboro, MD, USA*

Abstract:

Snowcover areal depletion curves inferred from the moderate resolution imaging spectroradiometer (MODIS) are validated and then applied in NASA's catchment-based land surface model (CLSM) for numerical simulations of hydrometeorological processes in the Kuparuk River basin (KRB) of Alaska. The results demonstrate that the MODIS snowcover fraction f derived from a simple relationship in terms of the normalized difference snow index compares well with Landsat values over the range $20 \leq f \leq 100\%$. For $f < 20\%$, however, MODIS 500 m subpixel data underestimate the amount of snow by up to 13% compared with Landsat at spatial resolutions of 30 m binned to equivalent 500 m pixels. After a bias correction, MODIS snow areal depletion curves during the spring transition period of 2002 for the KRB exhibit similar features to those derived from surface-based observations. These results are applied in the CLSM subgrid-scale snow parameterization that includes a deep and a shallow snowcover fraction. Simulations of the evolution of the snowpack and of freshwater discharge rates for the KRB over a period of 11 years are then analysed with the inclusion of this feature. It is shown that persistent snowdrifts on the arctic landscape, associated with a secondary plateau in the snow areal depletion curves, are hydrologically important. An automated method is developed to generate the shallow and deep snowcover fractions from MODIS snow areal depletion curves. This provides the means to apply the CLSM subgrid-scale snow parameterization in all watersheds subject to seasonal snowcovers. Improved simulations and predictions of the global surface energy and water budgets are expected with the incorporation of the MODIS snow data into the CLSM. Copyright © 2005 John Wiley & Sons, Ltd.

KEY WORDS Alaska; snow depletion curve; land surface modelling; MODIS; snow

INTRODUCTION

Given its prevalence in high-latitude and altitude regions, snow represents a key component of the global hydrological cycle. With its radiative and thermal properties, a snowcover greatly affects the overlying air and the underlying ground. Snow reflects most of the incident solar radiation owing to its elevated albedo (up to 80% or more), which leads to a suppression of near-surface atmospheric temperatures (Ellis and Leathers, 1998). The insulating properties of snow, owing to its relatively low thermal conductivity, determine to a large extent permafrost conditions (e.g. Stieglitz *et al*., 2001, 2003). Through sublimation processes, a snowcover constitutes a sink of energy near the surface and a source of atmospheric moisture (Déry *et al*., 1998; Déry

* Correspondence to: Stephen J. Déry, Program in Atmospheric and Oceanic Sciences, Princeton University, 307 GFDL, Princeton, NJ 08544-0710, USA. E-mail: sdery@princeton.edu

Received 23 December 2003
Accepted 25 May 2004

and Yau, 2002). During winter, snow acts as a temporary reservoir for water that may then be quickly released during the spring transition period, with meltwater contributing as much as 80% of the yearly discharge of some arctic streams and rivers (McNamara *et al*., 1998). Similarly, water resources for power generation and irrigation in many arid or semi-arid regions, such as the southwestern USA, depend largely on meltwater from alpine snowpacks (e.g. Sorooshian *et al*., 2002).

Recently, observational evidence has emerged suggesting ongoing changes in the state of seasonal snowcovers across North America and Eurasia. Brown and Braaten (1998) and Curtis *et al*. (1998) observed decreasing trends in snow depth, and Foster (1989) recorded trends towards an earlier spring snowmelt during the second half of the 20th century at Alaskan and Canadian arctic sites. In contrast, Ye *et al*. (1998) documented significant increases in snow accumulation in a zonal band between 60 and 70°N in northern Russia between 1936 and 1983. Changes in snowcover conditions are in part symptomatic of warmer near-surface air temperatures (Chapman and Walsh, 1993) that have led to modifications in continental precipitation patterns and phases (solid and liquid). These changes have important implications for all components of the global climate system, including the biosphere, cryosphere, and hydrosphere. For instance, enhanced wintertime snowfall in northern Russia has been observed to delay the spring melt, the onset of the growing season (Vaganov *et al*., 1999), and to increase river discharge to the Arctic Ocean (Peterson *et al*., 2002). An early onset of the spring melt in many regions of North America has prolonged the growing season such that the net primary production of vegetation has increased in recent years (e.g. Myneni *et al*., 1997).

Although significant improvements have recently been achieved in the simulation of the large-scale (from 10 to 1000 km) spatial distribution of snow (e.g. Stieglitz *et al*., 2001; Sheffield *et al*., 2003), typical land surface models (LSMs) applied in regional climate models (RCMs) and general circulation models (GCMs) usually consider the snowcover to be spatially uniform within a model grid cell that often covers an area greater than 1000 km^2. In nature, however, considerable variability in snowcover characteristics (snow depth, snow water equivalent, albedo, etc.) exists owing to small-scale variations in topography, vegetation, and meteorological conditions. For instance, snowdrifts on the North Slope of Alaska may contain up to 20 times more mass than snow in non-drift regions (Sturm *et al*., 2001). Thus, subpixel variability in snowcover can delay the onset of snow ablation from 2 weeks up to 2 months, with significant implications for the surface energy and water budgets (Arola and Lettenmaier, 1996; Luce *et al*., 1998; Stieglitz *et al*., 1999; Déry *et al*., 2004).

We demonstrate the feasibility of using remote-sensing data of snowcover area to improve numerical simulations of land surface processes in an Alaskan watershed. Snowcover measurements inferred from the moderate resolution imaging spectroradiometer (MODIS) are first validated using an independent dataset. Then, snow areal depletion curves, defined here as the temporal evolution of the snowcover fraction for a given area (Hall and Martinec, 1985), are inferred from MODIS and provide the constraints for a subgrid-scale snow parameterization that has recently been developed for NASA's catchment-based LSM (CLSM; Koster *et al*., 2000; Ducharne *et al*., 2000). The goals of this study are twofold: (1) to validate the representation of subpixel snow by MODIS in the Kuparuk watershed and to correct the data for possible biases; (2) to apply the MODIS snow areal depletion curves to constrain the free parameters introduced by the CLSM subgrid-scale parameterization and to determine the benefits (if any) of using this information in numerical simulations of land surface processes in Alaska. To achieve these objectives, snowmelt for an 11 year period over the Kuparuk River basin (KRB) on the North Slope of Alaska is investigated.

BACKGROUND

Although snow seasonally can cover up to 40% or more of the Northern Hemisphere land surface (Hall, 1988), its distribution and characteristics vary considerably even over small scales (on the order of tens of metres). For example, the KRB is located near 70°N, 150°W and covers an area of 8400 km^2 on the North Slope of Alaska (Figure 1). It is a watershed with its source in the Brooks Range and that extends 200 km to the north where the Kuparuk River discharges into the Arctic Ocean. For 8 months each year, the KRB is subject to a

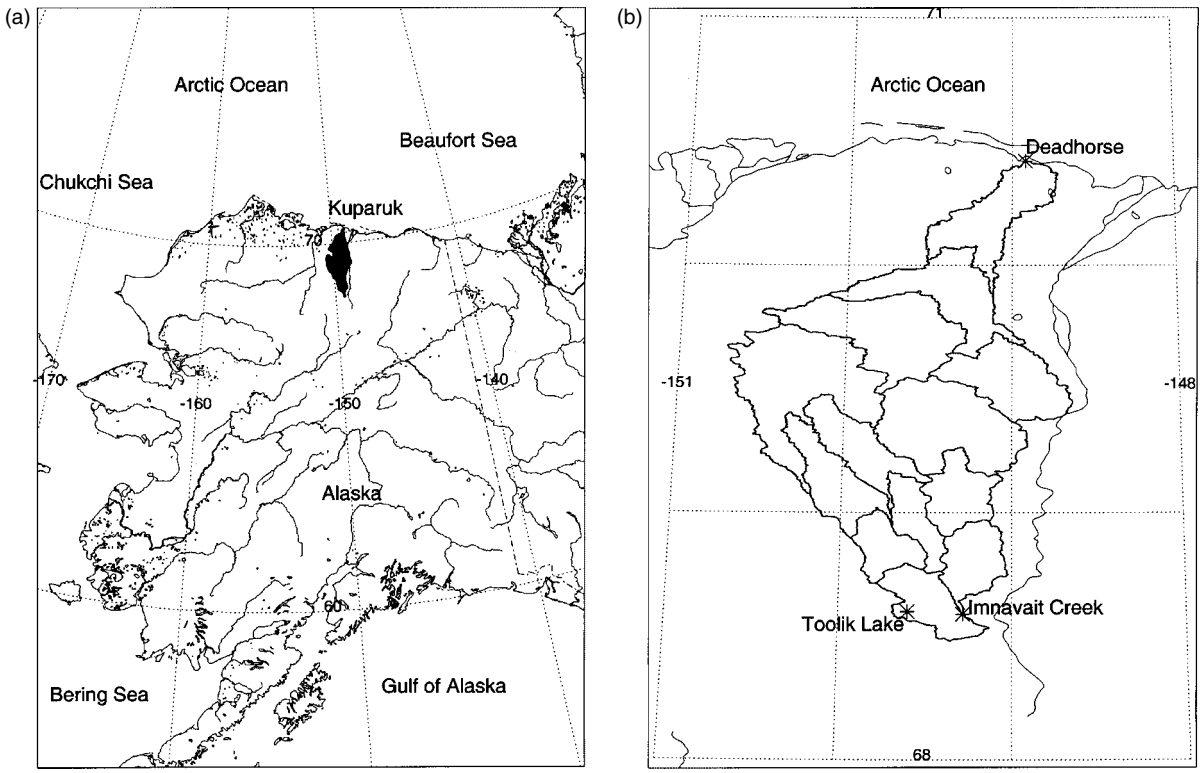

Figure 1. (a) Map of Alaska and surrounding features, including the KRB (shaded in black). (b) Close-up map of the KRB with locations identified in the text. Thirteen subbasins over which the CLSM is run are also outlined

seasonal snowcover that exhibits considerable small-scale, end-of-winter variability (Holmgren *et al.*; 1975, Kane *et al.*, 2000; Déry *et al.*, 2004). During a typical winter, a mean annual total of about 120 mm snow water equivalent (SWE) of solid precipitation accumulates on the surface of the KRB (McNamara *et al.*, 1998). Mesoscale and synoptic-scale atmospheric processes and patterns that govern storm tracks and the location of the arctic front first determine the exact amount of winter precipitation and its distribution on the North Slope of Alaska (Serreze *et al.*, 2001). Altitudinal control over precipitation type and intensity in the foothills of the Brooks Range further enhances the heterogeneous nature of the snowcover. In addition, frequent blowing snow events lead to considerable small-scale variability in the snowcover of the KRB (Déry and Yau, 1999).

Following the long period of formation (~8 months), multiple factors control the rapid ablation of the snowcover that typically occurs each May or early June. Snowmelt on the North Slope of Alaska is radiatively driven (Zhang *et al.*, 2001). The distribution and properties of the snowcover, including its depth, density, and heat content, also set the stage for the melting process (Lynch *et al.*, 1998). Zhang *et al.* (1996) propose that, during spring, longwave radiation from low-level clouds accelerates the melting process. Southward-facing slopes, where solar radiation is enhanced, ablate at a faster pace than northward-facing slopes (Déry *et al.*, 2004). The presence of vegetation protruding through the snowcover also locally accelerates the snowmelt process (Holmgren *et al.*, 1975). As the snowcover becomes patchy, the horizontal advection of heat promotes further melt (Liston, 1995). Despite this, persistent snowdrifts often remain on the arctic landscape 1 month after the onset of melt in non-drift regions (Holmgren *et al.*, 1975; Sturm *et al.*, 2001; Déry *et al.*, 2004). Field observations, photographs, remote-sensing data, and numerical modelling of the end-of-winter snowcover distribution on the North Slope of Alaska show that these features are small-scale phenomena with typical

lengths of tens to hundreds of metres (Sturm *et al*., 2001; Li and Sturm, 2002; Déry *et al*., 2004). Despite their relatively small sizes, snowdrifts in the region often attain thicknesses and water contents 3–20 times larger than observed in non-drift areas (Sturm *et al*., 2001). Thus, snow areal depletion curves in the KRB show a rapid decrease from 100% in the early stages of the melt period, followed by a slow progression toward a completely bare surface (Liston, 1999). The small-scale spatial distribution of snowcover, therefore, has significant control over snowmelt, with subsequent implications for the surface energy and water budgets during the spring transition period.

Snowdrift features have been documented in many other regions, including the Canadian Prairies and United States Great Plains (Pomeroy and Gray, 1995), as well as in the Western Cordillera (Luce *et al*., 1998). Although snowdrifts come in various shapes and sizes, they are usually elongated along one axis, with widths several times smaller than the distance they cover along their principal axis (Andreas, 1995). Although the larger snowdrifts tend to contain more SWE than their smaller counterparts, they appear less frequently on the landscape. Hence, both small and large snowdrifts have the potential to alter the surface energy and water budgets significantly. However, the degree to which this small-scale heterogeneity affects the large-scale climate remains unknown. As the global climate is changing, and as demands for freshwater continue to increase, the accurate simulation and prediction of the interactions and feedbacks between the land surface (including snowcover) and the atmosphere across all scales become essential.

NUMERICAL MODEL AND EXPERIMENTAL STRATEGY

Numerical model

The CLSM has been developed in conjunction with NASA's Seasonal-to-Interannual Prediction Project (NSIPP) to provide the boundary conditions for land surface fluxes of heat and moisture in the NSIPP GCM. By using the catchment as the fundamental hydrological unit, the CLSM is unique in simulating land surface processes (Ducharne *et al*., 2000; Koster *et al*., 2000). Instead of the rectangular grid cells commonly employed in conventional LSMs, the CLSM partitions the Earth's land surface into multiple drainage basins, each covering an area of about 5000 km^2. For example, the CLSM partitions the surface of Alaska into nearly 300 river basins, including the KRB.

The CLSM incorporates information derived from digital elevation models (DEMs), since it is topographically driven. While conserving mass and energy, the model simulates a wide range of land surface processes, including evapotranspiration, water infiltration, and river runoff. At high latitudes and altitudes, the CLSM must also represent snow and permafrost processes. To that end, the CLSM was coupled to a snow physics model and a permafrost dynamics module (Lynch-Stieglitz, 1994; Stieglitz *et al*., 2001). This version of the CLSM was shown to improve the simulation of ground temperatures and the subsequent location of the southern permafrost boundary across the North American continent. Despite the improved simulations of snow and ice processes at large scales (Stieglitz *et al*., 2001), the standard CLSM remains deficient in representing some of the small-scale snow heterogeneity found in nature. Since the spring transition period constitutes the most significant hydrological period on an annual basis in most high-latitude and -altitude river basins (Woo, 1986), there is a marked interest in simulating the timing and intensity of this event with a high level of accuracy. Thus, for the CLSM, a subgrid-scale snow parameterization has been developed. This parameterization divides the snowcover into two regions: one depicting a shallow snowcover area A_{shallow}, where winds erode snow from the surface, and another representing a deep snowcover area A_{deep}, where winds deposit the snow. The shallow snow fraction denotes flat terrain or windward slopes where winds easily transport snow, whereas the deep snow fraction represents valleys and leeward slopes where snow preferentially accumulates. Since blowing snow is the dominant process causing snowcover heterogeneity, Déry *et al*. (2004) demonstrated that this parameterization significantly improves the simulation of snowcover ablation and of river runoff for the Upper KRB, a 142 km^2 subbasin of the KRB. Values of the shallow (0·65) and deep (0·35) snowcover fractions were chosen based on results from the Piektuk blowing snow model (Déry and Taylor, 1996; Déry

et al., 1998) applied to a north–south transect in the Upper KRB. To avoid the computational demands of a distributed blowing snow model, it is demonstrated later in this paper that remote-sensing data of snowcover area can also be utilized to infer the values of A_{shallow} and A_{deep}.

Model modifications

Apart from its contribution to subgrid-scale spatial variability, blowing snow enhances surface latent heat fluxes during high wind and relatively dry atmospheric conditions (Déry and Yau, 2001a). Aeolian snow sublimation is parameterized in the updated CLSM following Déry and Yau (2001b) and is computed when ambient conditions are favourable for blowing snow (Déry and Yau, 1999, 2002). The additional latent heat arising from aeolian sublimation occurs over the shallow snowpack area where winds are able to scour snow from the surface.

A deep snowpack area forms in riverine depressions owing to snow redistribution. In turn, this creates snow damming of meltwater that delays the onset of significant runoff during the spring transition period (Kane *et al*., 2000). In the CLSM subgrid-scale snow parameterization, meltwater from the shallow snowpack area is transferred to the deep snowpack area instead of contributing directly to ground infiltration and/or surface runoff. Snow damming effects retard the onset of peak runoff rates during the spring transition season.

Two novel features incorporated in this version of the CLSM affect the responsiveness of soils to precipitation. The first is the inclusion of stormflow processes in the model by allowing for shallow subsurface flow ('quickflow') from near-saturated soil that is located above the main water table to contribute directly to surface runoff (Shaman *et al*., 2002). The second is the subgrid-scale spatial variability of the depth-to-bedrock that considers the effects of shallow (deep) soils in highland (lowland) regions within a catchment. This feature becomes important as the active layer deepens and a greater fraction of the soil column becomes hydrologically active. The integration of these two features leads to improved simulations of runoff responsiveness (Shaman *et al*., 2002).

Experimental strategy

Instead of interacting with the NSIPP GCM, the CLSM is run offline over the KRB for the period 1991–2001. During the spring transition period, there is a rapid expansion of saturated soil areas on the Arctic Coastal Plain, since small lakes and wetlands capture part of the meltwater (Bowling *et al*., 2003). The KRB, therefore, is partitioned into 13 separate subbasins of about 650 km^2 to better capture the effects of local topography and of local meteorological conditions on hydrological processes in the basin (Figure 1b). A DEM with a 25 m horizontal resolution is used to generate a probability density function of topographic parameters for each of the 13 subbasins that are used as input in the CLSM. In each of the 13 subbasins, the model is driven by a meteorological dataset constructed from observations recorded at 18 stations within the KRB. The atmospheric fields that force the CLSM are the hourly observed air temperature, humidity, precipitation, wind speed, surface atmospheric pressure, and incoming longwave and shortwave radiative fluxes. The CLSM is first spun up over a period of 30 years to equilibrium using 1991 observational data recursively. The model is then integrated forward in time until 31 December 2001. A timestep of 20 min is used in all integrations. Simulations with and without the subgrid-scale snow parameterization are presented to illustrate the benefits (if any) of incorporating the MODIS snowcover data into the simulations. Four supplemental simulations are then conducted to test the sensitivity of the results to the recent modifications incorporated into the CLSM (see previous section). For each simulated year, the focus is on the spring transition period, such that results for river runoff and SWE are presented for May and June only.

MODIS SNOWCOVER PRODUCTS

Space-borne instruments have the advantage of providing global or hemispheric snow maps at high resolutions. Among recent satellites mounted with instruments that have snow detection capabilities are the Earth

Observing System (EOS) Terra and Aqua spacecraft, launched in 1999 and 2002 respectively. Both Terra and Aqua carry a MODIS instrument that probes the Earth's atmosphere and surface using 36 visible and thermal infrared channels (Barnes *et al.*, 1998). Based on heritage algorithms developed using aircraft and Landsat data (Crane and Anderson, 1984; Dozier, 1989), MODIS band 4 (0·545–0·565 μm) and band 6 (1·628–1·652 μm) measurements of reflectance, the normalized difference snow index (NDSI) is evaluated (Hall *et al.*, 1995; 2002a):

$$\text{NDSI} = \frac{\text{band 4} - \text{band 6}}{\text{band 4} + \text{band 6}} \tag{1}$$

A pixel where NDSI >0·4 and where reflectance in MODIS band 2 (0·841–0·876 μm) is >11% is identified as snow. To prevent the erroneous classification of dark targets as snow, however, a grid point is not classified as snow if MODIS band 4 reflectance is <10%, even if the other criteria are met. In addition to NDSI, MODIS bands 1 (0·620–0·670 μm) and 2 (0·841–0·876 μm) are used to calculate the normalized difference vegetation index (NDVI) from

$$\text{NDVI} = \frac{\text{band 2} - \text{band 1}}{\text{band 2} + \text{band 1}} \tag{2}$$

Following the methodology of Klein *et al.* (1998), an additional test using the NDSI and NDVI is then used to improve the detection of snow in dense forests. An 'impossible snow mask' is also implemented to decrease the errors of commission in warm areas where clouds and/or dense aerosols and smoke, for example, may cause the MODIS algorithm to map snow erroneously. Cloud (Ackerman *et al.*, 1998) and land/water masks supply the final criteria used in the generation of MODIS snowcover maps. This automated snow mapping algorithm yields hemispheric snowcover charts that complement existing operational maps (e.g. Ramsay, 1998; Hall *et al.*, 2002b), while providing significant advances in spatial resolution and snow/cloud discrimination capabilities. An important consideration for this study is the daily coverage of the land surface by MODIS, since snowcover conditions change rapidly from day to day during the spring transition period in Alaska. Furthermore, ongoing validation studies demonstrate that the MODIS snow maps compare favourably with operational snow charts (Hall *et al.*, 2002a,b; Klein and Barnett, 2003; Maurer *et al.*, 2003).

MODIS snowcover products are available at temporal resolutions varying from 1 to 8 days and at spatial resolutions varying from 500 m to 0·05° (~5·6 km at the equator) (Hall *et al.*, 2002a). Even at a spatial resolution of 500 m, however, binary (snow/no snow) MODIS products of snowcover area exhibit some deficiencies in depicting actual snow conditions owing to the small-scale nature of snowdrifts (see Background section) and variations in topography. To improve the representation of land surface heterogeneity, several relationships between the NDSI and snowcover area have been formulated to detect the fractional coverage of snow for each MODIS 500 m pixel (e.g. Kaufman *et al.*, 2002; Vikhamer and Solberg, 2002). Salomonson and Appel (2004) compared MODIS data with Landsat satellite imagery at a spatial resolution of 30 m that was considered to be ground truth. For the North Slope of Alaska, they find that the snow areal fraction f [0–1] within a 500 m MODIS pixel can be estimated from

$$f = A + B \times \text{NDSI} \tag{3}$$

where $A = 0{\cdot}06$ and $B = 1{\cdot}21$. The linear regression attains an overall accuracy of $R^2 = 0{\cdot}95$. In the following section, this methodology is validated for the KRB during 2 days in the spring transition period of 2002. The results are then applied to generate snow areal depletion curves and to constrain the CLSM parameters for subgrid-scale snow.

METHODS: VALIDATION AND APPLICATION OF MODIS SNOWCOVER DATA

Before application in simulations of land surface processes, MODIS snowcover data are first validated against Landsat imagery of the North Slope of Alaska. Snow areal depletion curves deduced from the MODIS data

are then presented and are used to infer the shallow and deep snowcover fractions in the KRB. These fractions are applied in the CLSM subgrid-scale snow parameterization and the model is integrated over a period of 11 years to simulate land surface processes over this catchment.

Validation of MODIS snowcover data

During 2002, snowmelt in the KRB was initiated in mid-May and lasted about 2 weeks. Figure 2a presents hourly surface air temperature measurements recorded at the Arctic Long Term Ecological Research (LTER) station at Toolik Lake, Alaska (see Figure 1b). Meteorological conditions at the Arctic LTER, representative of the entire KRB, suggest that surface air temperatures climb above the freezing point on 16 May 2002 and that the relatively warm conditions persist for 10 days. Snow-course surveys conducted by Kane and Hinzman (2003) at Imnavait Creek, a 2·2 km^2 watershed situated in the headwaters of the KRB, reveal the rapid melt that accompanied the above-freezing temperatures during the week of 15–22 May 2002 (Figure 2b). Subsequent to this, measurements of freshwater discharge near the mouth of the Kuparuk River collected at Deadhorse by the USGS exhibit a crest on 26 May 2002 associated with the meltwater (Figure 2b). By the end of the month, river runoff rates abate and snowmelt is nearly complete across the entire KRB.

Owing to the high frequency of blowing snow events in the KRB, the snowcover displays considerable heterogeneity even in midwinter. However, since MODIS provides information only on the snowcover fraction, we choose two dates during the snowmelt period of 2002 for which MODIS and Landsat data are available and when mostly clear skies are observed: 23 May 2002, approximately midway during the snowmelt, and 30 May 2002, near the end of the melt period. For these cases, Landsat binary measurements of snowcover at a spatial resolution of 30 m are binned to pixels of 500 m and the corresponding MODIS subpixel snowcover fraction is inferred from Equation (3). The comparisons are performed only over the domain of the KRB.

Figure 3 presents a comparison of MODIS and Landsat snowcover fraction for each 500 m pixel in the KRB. For the two dates, MODIS values of f compare favourably with those from Landsat. The mean absolute

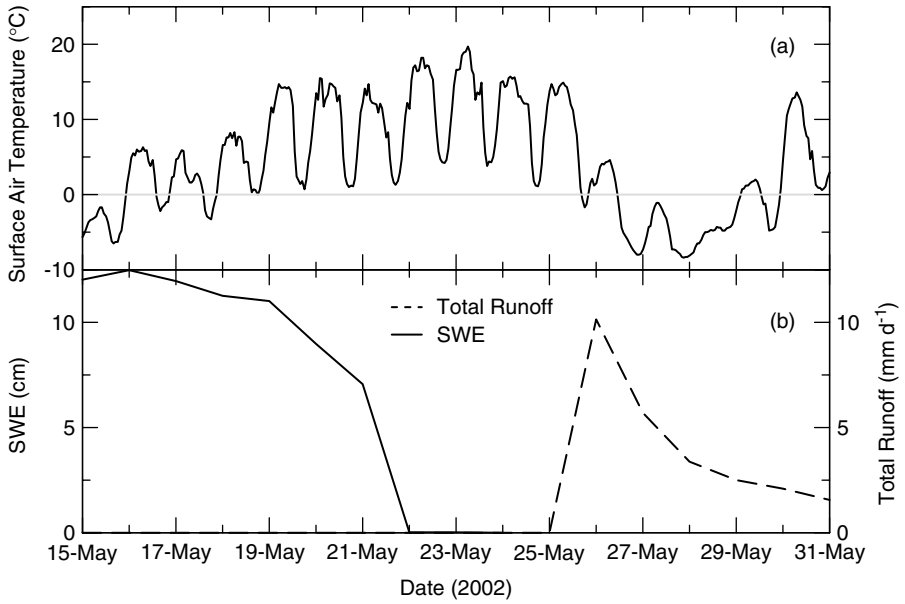

Figure 2. (a) Hourly values of surface air temperature recorded at Toolik Lake between 15 and 31 May 2002. (b) Daily values of the observed SWE at Imnavait Creek and of total runoff rates recorded at Deadhorse, near the mouth of the Kuparuk River. Measurements of surface air temperature are from the Arctic LTER database (http://ecosystems.mbl.edu/arc/), the SWE data are from Kane and Hinzman (2003), and the discharge data are from the United States Geological Survey (USGS)

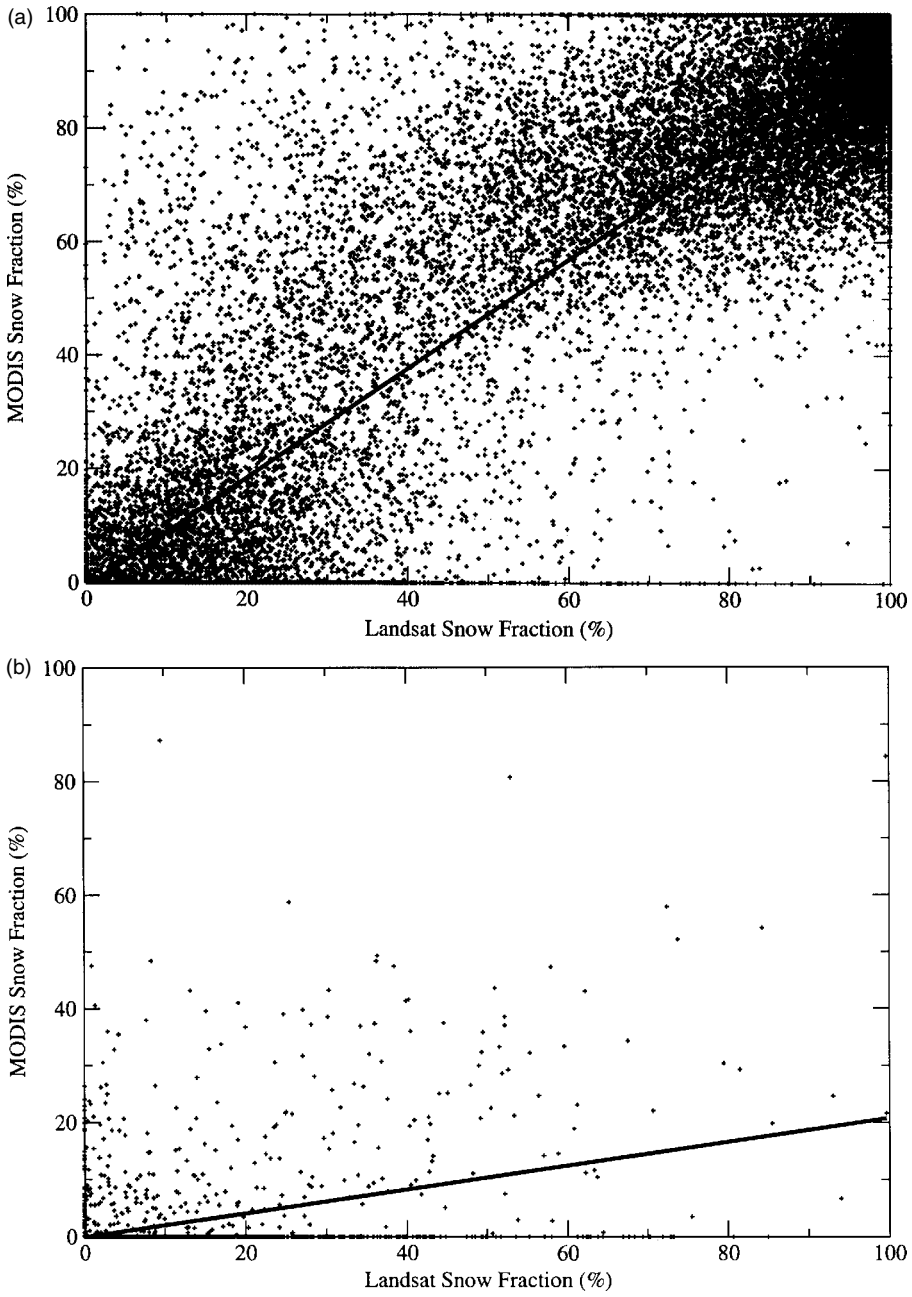

Figure 3. A comparison of Landsat versus MODIS snowcover fraction at 500 m resolution. The MODIS fractional data are derived from a linear regression that relates subpixel snowcover fraction to values of the NDSI. This comparison is conducted over the KRB on (a) 23 May 2002 and (b) 30 May 2002. The thick black lines denote linear regressions performed on the data

errors in snowcover fraction are 8·7% and 2·1% on 23 and 30 May 2002 respectively (Table I). However, there is better correspondence between the two datasets early on during the melt period, as evidenced by the respective values of 0·89 and 0·19 for the coefficients of determination R^2. The higher mean absolute and root-mean-square errors obtained during the early melt period arise from the greater range in the snowcover

Table I. Results from the error analysis[a]

Date	Pixels	R^2	MAE (%)	RMSE (%)	f_{Landsat} (%)	f_{MODIS} (%)
23 May 2002	35 022	0·89	8·7	13·9	40·0	37·6
30 May 2002	13 413	0·19	2·1	6·5	2·2	0·4
Total	48 435	0·90	6·9	12·3	—	—

[a] R^2: coefficient of determination; MAE: mean absolute error; RMSE: root-mean-square error; f_{Landsat}: Landsat snow-cover fraction; f_{MODIS}: MODIS snow-cover fraction.

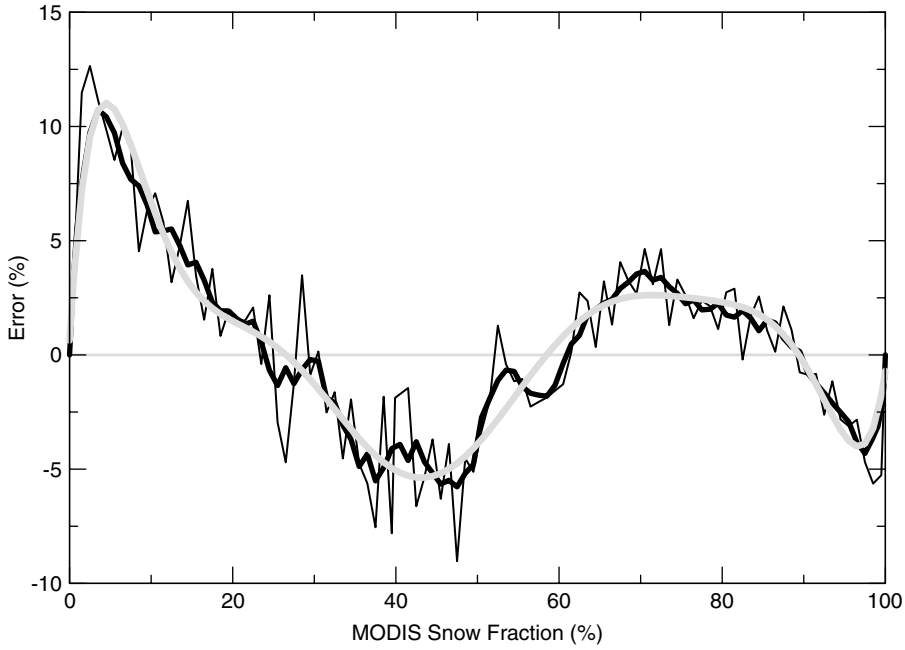

Figure 4. The error in the MODIS subpixel snow fraction compared with the Landsat data. The data were binned into 100 intervals, each covering a 1% snow fraction. This comparison is conducted over the KRB and uses data from both 23 May and 30 May 2002. The thick black line denotes a five-point running mean and the grey line is a ninth-order polynomial fit to the data

fraction observed at that time. Overall, we obtain errors that are similar to those reported by Salomonson and Appel (2004) for the same region, with $R^2 = 0{\cdot}90$, a mean absolute error of 7% and a root-mean-square error of 12% in snowcover fraction.

A more detailed error analysis of the data presented in Figure 3 is now performed. Figure 4 reveals the error in 100 snow-fraction bins, each covering 1% in area, between the Landsat and MODIS snow fractions. This analysis shows that MODIS represents well the Landsat snow fraction (±5%) over a wide range of snow-fraction values (20 to 100%). However, MODIS tends to underestimate the snow fraction when the snowcover becomes patchy ($f < 20\%$), with errors reaching 13%. A ninth-order polynomial fit to the errors, given by

$$E = a_0 + a_1 f + a_2 f^2 + a_3 f^3 + a_4 f^4 + a_5 f^5 + a_6 f^6 + a_7 f^7 + a_8 f^8 + a_9 f^9 \quad (4)$$

provides a function by which these biases can easily be removed. Coefficients for Equation (4) are provided in Table II.

Table II. Coefficients for the polynomial fit (Equation (4))

Coefficient	Value	Coefficient	Value
a_0	$6{\cdot}3076 \times 10^{-1}$	a_5	$1{\cdot}1081 \times 10^{-4}$
a_1	5·9015	a_6	$-1{\cdot}7491 \times 10^{-6}$
a_2	−1·1474	a_7	$1{\cdot}6351 \times 10^{-8}$
a_3	$9{\cdot}4558 \times 10^{-2}$	a_8	$-8{\cdot}3401 \times 10^{-11}$
a_4	$-4{\cdot}2263 \times 10^{-3}$	a_9	$1{\cdot}7892 \times 10^{-13}$

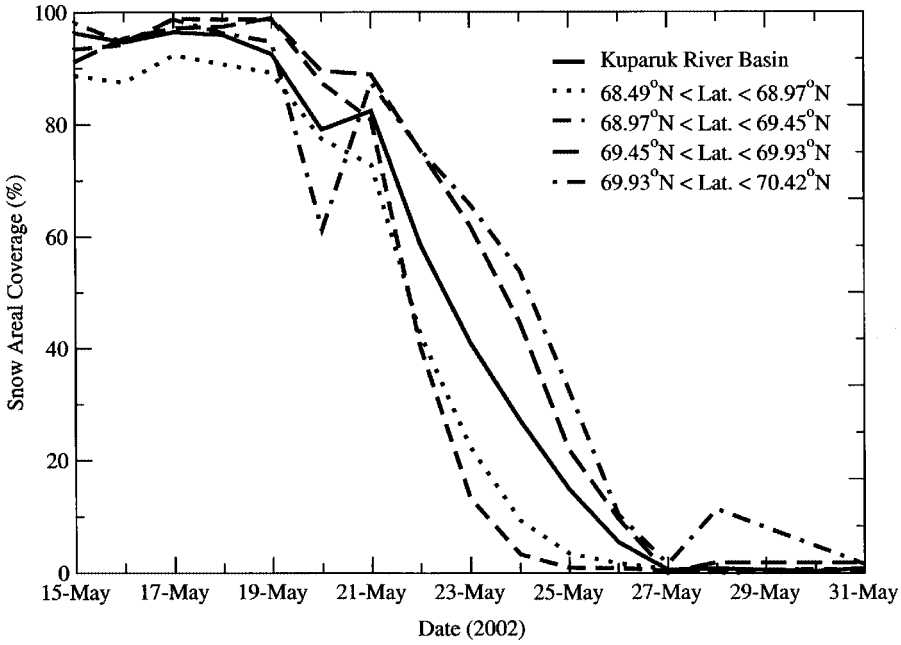

Figure 5. The temporal evolution of snow areal coverage deduced from MODIS over the KRB (black line) between 15 and 31 May 2002. Additional snow areal depletion curves, representing four zonal bands of 0·5° within the KRB, are also included

Snow areal depletion curves inferred from MODIS

MODIS imagery providing the best daily nadir coverage (usually near local noon) is selected to construct a snow areal depletion curve for the KRB during 2002. Daily values of the snowcover fraction are computed using only clear-sky pixels; hence, the total number of MODIS cells used in the estimates varies on a daily basis, but cloudy regions do not influence the results. More uncertainty in snowcover fractions for the KRB exists during cloudy periods, and this limitation in our methodology is covered in the Discussion section.

Based on the daily uncorrected MODIS subpixel data, the snow areal depletion curve for the spring transition period of 2002 over the domain of the KRB is presented in Figure 5. This suggests that the onset of melt was initiated near 19 May 2002 and lasted about 10 days, consistent with the measurements of river discharge rates at Deadhorse and of SWE at Imnavait Creek (see Figure 2b). Often, the onset of melt is initiated in the southern sections of the basin, where solar radiation is greatest. Figure 5 also presents the snow areal depletion curves in four latitudinal bands of about 0·5° each within the KRB. This shows that a time lag of several days exists in the melt of snow in the most northern regions of the basin compared with their southern counterparts. The latitudinal gradient in snowmelt may also explain the delay in the observed peak in the hydrograph compared with the evolution of snowcover area.

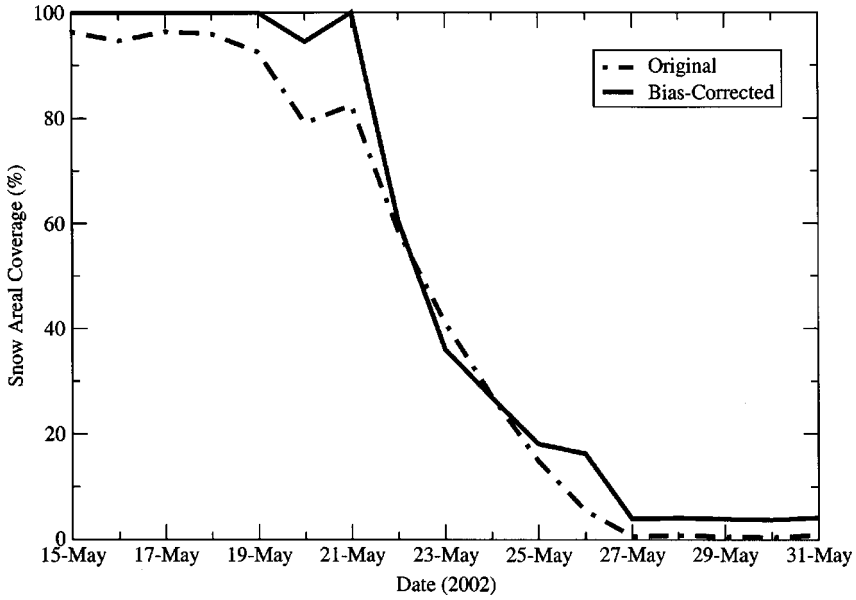

Figure 6. The temporal evolution of snow areal coverage inferred from the original and the bias-corrected MODIS data over the KRB in May 2002

There is one notable contrast between the snow areal depletion curves derived from the uncorrected MODIS data and those obtained from snow-course measurements. Liston (1999) presented a comprehensive set of snow observations for Imnavait Creek. The observed snow areal depletion curve (Liston, 1999: Figure 3c) shows that, in the late stages of the spring melt, there is a fraction (~5–10%) of snow remaining within the Imnavait Creek watershed. This is attributed to snowdrifts that persist on the arctic landscape for several weeks as they slowly ablate, whereas the remainder of the shallow snowcover has already vanished. The scale of these features and the detailed error analysis suggest that snowdrifts are not being detected by MODIS (see Background and Validation of MODIS snowcover data sections). In fact, snow areal depletion curves derived from MODIS show little, if any, snow persisting throughout the KRB during the spring transition period of 2002 (Figure 5).

Figure 6 depicts the snow areal depletion curve when these errors are removed from the MODIS snow fractions. Here, the new MODIS snow fraction f_{new} is obtained by adding the error E to the old snow fraction f_{old} for a given MODIS snow fraction, i.e. $f_{\text{new}} = f_{\text{old}} + E(f_{\text{old}})$, where E is estimated from the polynomial fit (Equation (4)). The bias-corrected snow areal depletion curve now shows the persistent snowdrifts (covering ~5% of the KRB, or equivalent to the same ratio observed by Liston (1999) at Imnavait Creek) that remain on the arctic landscape as a result of wind redistribution.

A method for partitioning the KRB into shallow and deep snowcover fractions

To obtain the fractions covered by shallow and deep snowpacks within the KRB, the following procedure is used. On the bias-corrected snow areal depletion curve, two tangents are drawn (Figure 7). One tangent is associated with the point at which the slope of the snow areal depletion curve attains its maximum absolute value, and the other is associated with the point where the slope of the snow areal depletion curve lessens to a threshold absolute value of 1% per day after the maximum absolute value has been achieved. (The physical basis for the selection of these two points along the snow areal depletion curve is covered in the Discussion section.) The intersection of these two tangents provides the day, as denoted by the vertical dashed line in Figure 7, at which time the shallow snowpack is assumed to have completely melted. The remainder of the

snowpack is taken as the deep area. Based on this methodology, $A_{shallow} = 76\%$ and $A_{deep} = 24\%$ for this case. A similar procedure is used to obtain the shallow and deep snowcover fractions in each of the four zonal bands considered in Figure 5. Table III shows that there is more snowcover heterogeneity in the southern sections of the KRB, where greater topographic variations exist. Thus, the shallow snowcover fraction ranges from 0·20 along the coast to 0·27 in the headwaters of the KRB. This is in accord with the previous findings of Déry *et al*. (2004), who used a blowing snow model to infer a shallow snowcover fraction of 0·35 for the Upper KRB (see Numerical model section). The MODIS deep and shallow snowcover fractions are then incorporated into the CLSM subgrid-scale snow parameterization for simulations of hydrometeorological processes in the KRB. Since MODIS is a recent initiative, the shallow and deep snowcover fractions are assumed constant from year to year in the numerical simulations. Further comparisons between MODIS and Landsat data will be required to demonstrate that there is little interannual variability in the shape of the snow areal depletion curves in the KRB.

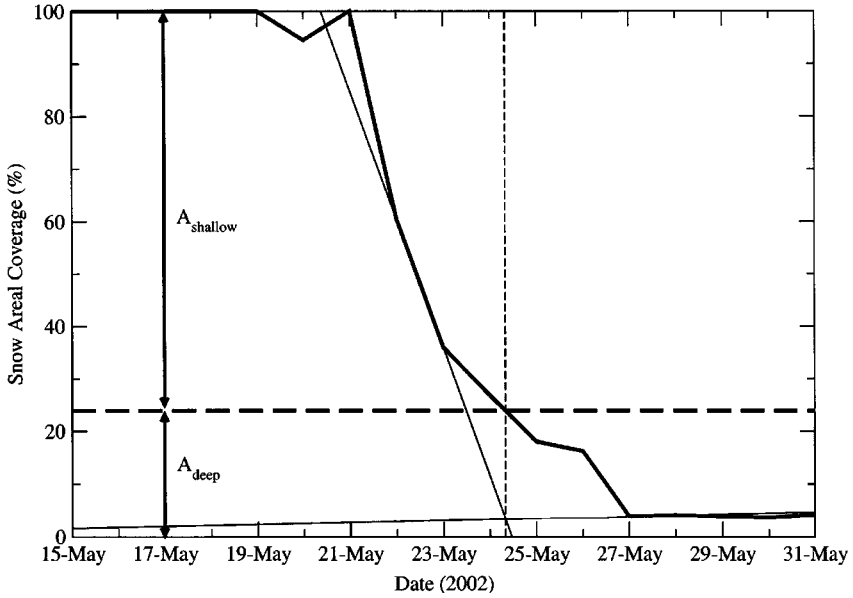

Figure 7. The temporal evolution of snow areal coverage inferred from the bias-corrected MODIS data over the KRB in May 2002 (thick black line). The text describes the methodology by which the areas covered by a shallow ($A_{shallow}$) and a deep (A_{deep}) snowcover are inferred from the snow areal depletion curve

Table III. Shallow and deep snow-cover fractions ($A_{shallow}$ and A_{deep} respectively) for four latitudinal bands in the KRB

Latitudinal band	$A_{shallow}$	A_{deep}
68·49 < Lat. <68·97 °N	0·73	0·27
68·97 < Lat. <69·45 °N	0·75	0·25
69·45 < Lat. <69·93 °N	0·79	0·21
69·93 < Lat. <70·42 °N	0·80	0·20

SIMULATION RESULTS

Simulations of land surface processes in Alaska using MODIS snowcover data

Results from two CLSM numerical simulations are now presented: one as the control (CTL) experiment without subpixel snow heterogeneity (i.e. with a spatially uniform snowcover) and another with the subgrid-scale snow (SSS) parameterization. In the SSS experiment, the shallow and deep snowcover areas are specified using the MODIS subpixel data for the nearest zonal band to each of the 13 subbasins as obtained in the previous section. The values of A_{shallow} and A_{deep} are assumed constant in time, as snow distributions are mostly driven by topographic variations in the KRB and, thus, show a high degree of correlation from year to year (König and Sturm, 1998). Emphasis is given to the evolution of the simulated river runoff and of snowpack ablation. Comparisons with field-based observations are conducted where an appropriate dataset is available.

Figure 8 presents a comparison of the observed and the simulated daily discharge rates for the Kuparuk River, with and without the subgrid-scale snow parameterization, between 1 May and 30 June for each of 11 years. Runoff data recorded by the USGS at Deadhorse near the mouth of the Kuparuk River allow an evaluation of the CLSM's performance over the entire watershed. From the observations, it is evident that runoff associated with snowmelt produces a crest in the hydrograph in late May or early June. The standard CLSM has difficulty capturing this peak, since it tends to overestimate the amount of water associated

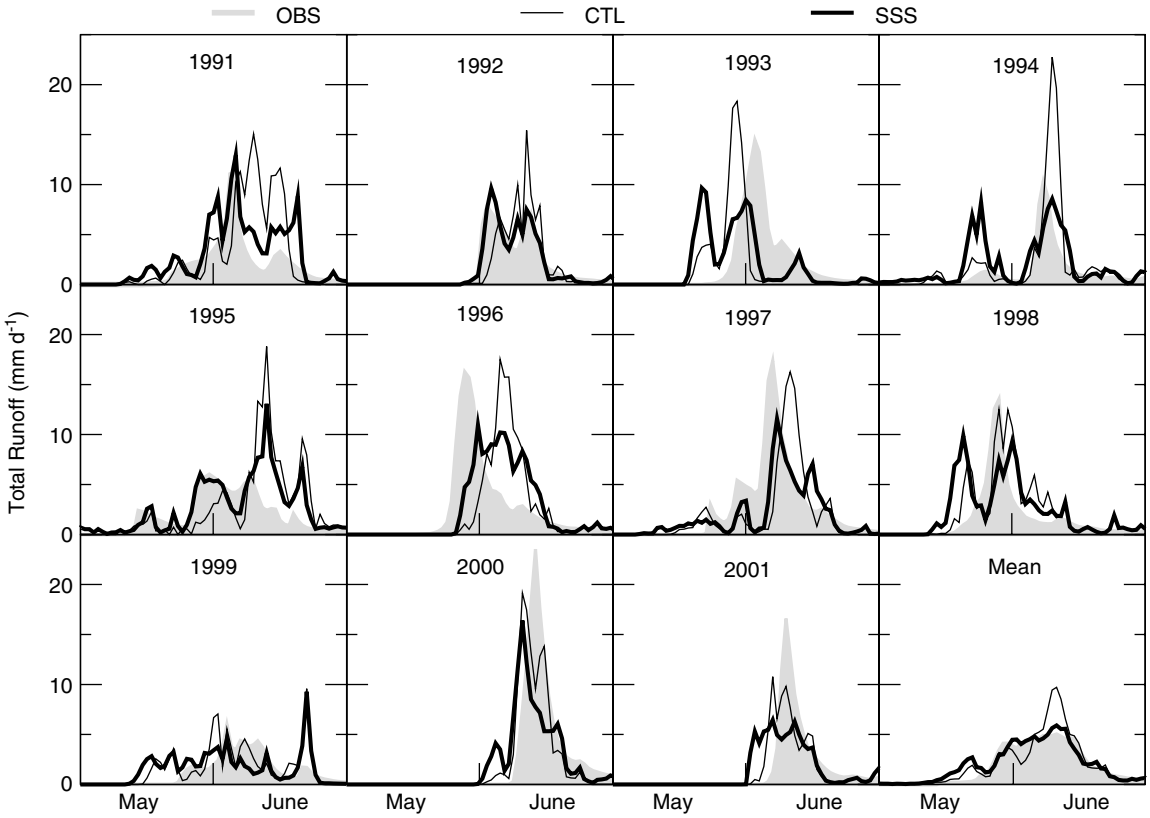

Figure 8. The observed (OBS) and simulated daily rates of total runoff for the Kuparuk River from 1 May to 30 June 1991–2001. Mean daily values of the observed and simulated runoff over the period 1991–2001 are also shown. Two simulations are conducted with the CLSM: one as the control (CTL) experiment without subpixel snow heterogeneity and another with the subgrid-scale snow (SSS) parameterization. River discharge measurements are from the USGS

with snowmelt. Without the subgrid-scale snow parameterization, the CLSM also has problems timing the peak discharge rates compared with observations. With the subgrid-scale snow parameterization, a significant improvement in the simulations is achieved. The CLSM is now able to capture with more accuracy the timing and the amount of river runoff associated with snowmelt.

The seasonal cycle of mean daily runoff rates also illustrates the improved results when the subpixel snow heterogeneity is considered in the CLSM. Compared with the 11 year average of the daily observed runoff, the CLSM attains coefficients of determination of 0·88 and 0·78 with and without the subgrid-scale snow parameterization respectively (Table IV). The SSS experiment yields a mean absolute error of 0·48 mm day^{-1} in river discharge, a reduction of 0·17 mm day^{-1} from the CTL simulation. A comparable decline in the root-mean-square error is also obtained with the updated model. This analysis suggests that there are significant benefits in incorporating the MODIS snowcover data for simulations of river runoff on the North Slope of Alaska.

Comprehensive snow-course surveys are not available for the KRB as a whole; thus, the simulated SWE for a single subbasin that includes the area covered by Imnavait Creek is chosen for the validation of snowcover evolution (see Figure 1b). There exists a long-term dataset of snow ablation data that has been collected each spring at Imnavait Creek as part of the Water and Environmental Research Center (WERC) of the University of Alaska Fairbanks' North Slope Hydrology initiative (Kane and Hinzman, 2003). Measurements of SWE are, therefore, available for the 11 year period chosen for the numerical simulations. A quantitative evaluation of the CLSM's performance is conducted with the point observations even though the simulations are for a basin that covers 424 km^2 in area.

The evolution of the observed and the simulated SWE, with and without the subgrid-scale snow parameterization, is shown in Figure 9. The snow-course surveys demonstrate that snowmelt occurs in May or early June, with melt lasting about 2 weeks on average before the complete disappearance of snow at Imnavait Creek. The CTL and SSS simulations capture reasonably well the end-of-winter amount of SWE recorded at Imnavait Creek, with the greatest discrepancies in 1995. When uniform snowcover conditions

Table IV. Error analysis for the CLSM simulations compared with observations (OBS)[a]

Variable	Experiment	Mean (mm day^{-1})	R^2	MAE (mm day^{-1})	RMSE (mm day^{-1})
Runoff	OBS	1·7	—	—	—
	CTL	2·1	0·78	0·65	0·50
	SSS	2·0	0·88	0·48	0·29
	ST1	2·0	0·88	0·48	0·29
	ST2	2·0	0·89	0·48	0·29
	ST3	2·0	0·87	0·49	0·29
	ST4	2·0	0·89	0·47	0·28
SWE	OBS	40	—	—	—
	CTL	51	0·74	19	3·7
	SSS	50	0·74	18	3·4
	ST1	52	0·74	20	3·7
	ST2	54	0·77	18	3·5
	ST3	50	0·74	18	3·4
	ST4	49	0·74	18	3·4

[a] The analysis is based on the mean daily values of river runoff and of SWE between 1 May and 30 June over the period 1991–2001 in the KRB. Observations of SWE are taken from Imnavait Creek (Kane and Hinzman, 2003) and are compared with the simulated SWE in the southernmost of 13 subbasins over which the CLSM is run. The simulated river runoff rates from all 13 subbasins are areally averaged and compared with the USGS measured values at Deadhorse. Two standard simulations are conducted with the CLSM: one as the control (CTL) experiment without subpixel snow heterogeneity and another with the subgrid-scale snow (SSS) parameterization. Results from four additional sensitivity tests are included, whereby the SSS simulation is modified to remove the effects of either blowing-snow sublimation (ST1), snow damming (ST2), the stormflow mechanism (ST3), or variations in depth-to-bedrock (ST4) (see text for details).

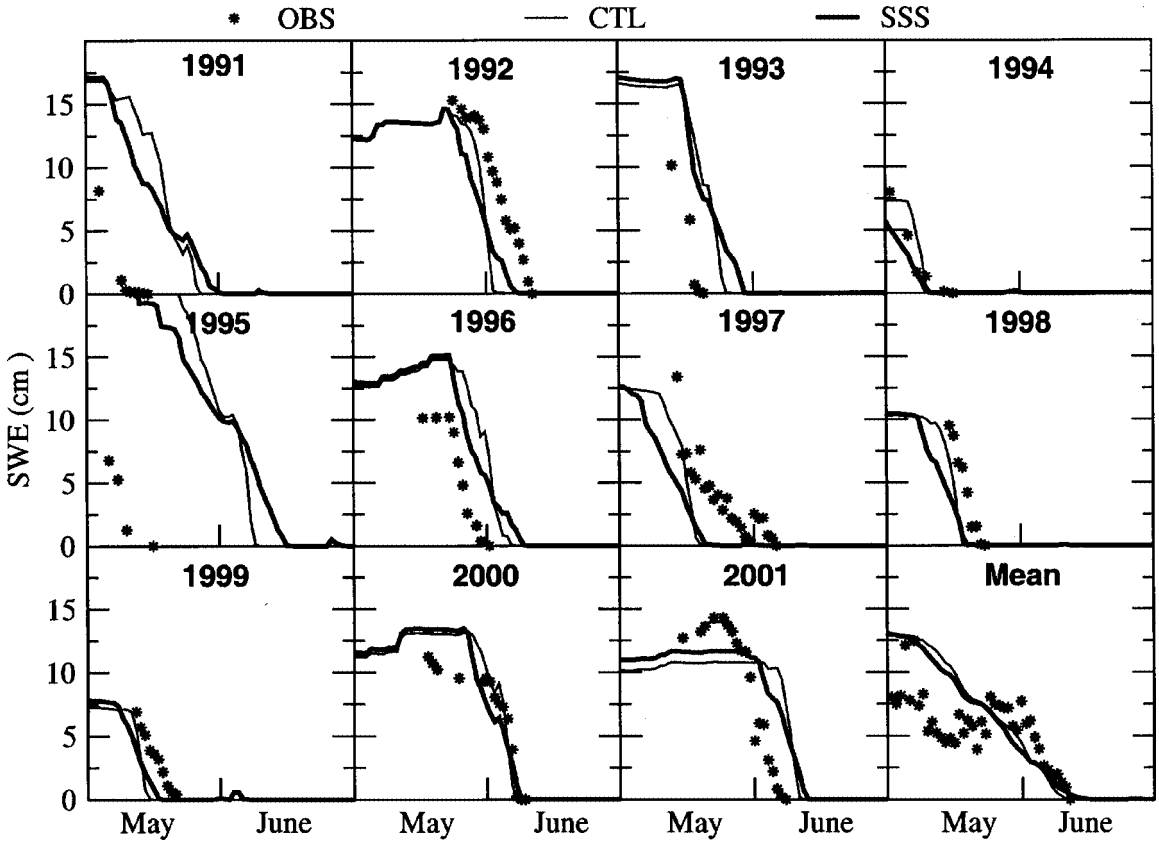

Figure 9. The observed (OBS) SWE from Imnavait Creek (Kane and Hinzman, 2003) compared with the simulated SWE in the southernmost of 13 subbasins over which the CLSM is run from 1 May to 30 June 1991–2001. Mean daily values of the observed and simulated SWE over the period 1991–2001 are also shown. Two simulations are conducted with the CLSM: one as the control (CTL) experiment without subpixel snow heterogeneity and another with the subgrid-scale snow (SSS) parameterization

are assumed in the CLSM, the snowpack collapses rapidly when melt is initiated. Once subgrid-scale snow heterogeneity is taken into consideration, the simulated ablation of SWE is more gradual and is more in line with the point observations from Imnavait Creek. In the SSS experiment, depletion of SWE is accelerated in the shallow snowcover fraction but delayed in the deep snowcover fraction, extending the melt period by a week or two compared with the CTL experiment.

An error analysis of the 11 year average of the daily simulated SWE for May and June shows that the CLSM attains a coefficient of determination of 0·74 in both the CTL and SSS experiments compared with the observations (Table IV). For the same time period, the mean absolute and root-mean-square errors are both reduced when the subgrid-scale snow parameterization, constrained by the MODIS data, is introduced into the CLSM.

Greater disparities between the observed and simulated SWE exist, since snowcover heterogeneity at Imnavait Creek represents local conditions only and does not necessarily describe actual conditions over the entire subbasin where the CLSM is run. Thus, increasing the spatial resolution of the SWE sampling at Imnavait Creek will not improve comparisons between observed and modelled snowcover conditions in this case (see Snow areal depletion curves inferred from MODIS section). Unless an aggregate of basinwide snow surveys or of satellite data is performed, a thorough validation of the modelled SWE in the KRB will remain elusive. Thus, validation of SWE using non-aggregated point observations remains a difficult process. This

also highlights the importance of river discharge as a validation product for large-scale land surface studies such as the one conducted here, since it represents an integrated response of the basinwide landscape.

Sensitivity tests

In the previous section, we demonstrated that the incorporation of subgrid-scale snow in the CLSM improves the representation of river runoff and of snowcover conditions during the spring transition period of the KRB. We now conduct additional simulations to test their sensitivity to other processes that are not resolved by the standard CLSM (see Model modifications section). Four supplemental simulations are performed in which the SSS simulation is modified to remove the individual impacts of (1) blowing snow sublimation (ST1), (2) snow damming (ST2), (3) the stormflow mechanism (ST3), and (4) variations in depth-to-bedrock (ST4) on the results. The sensitivity tests use the same experimental strategy as the SSS simulation, with the exception that the specified process is turned off during the integration.

Table IV includes results from four sensitivity tests in addition to the CTL and SSS simulations. The removal of the blowing-snow sublimation process from the SSS simulation increases the amount of snow that degrades the modelled SWE. Without snow damming, the simulated river runoff and SWE deviate little from the SSS experiment. The omission of the stormflow process and of the subgrid spatial variability in depths-to-bedrock also has little impact on the SSS simulation.

Overall, the sensitivity tests show that the small-scale snowcover heterogeneity has the most significant impact on the simulation of SWE and of river runoff in the KRB. Blowing-snow sublimation, snow damming, the stormflow process, and the spatial variability of depths-to-bedrock have secondary impacts on the simulated water budget variables for the KRB. Processes currently not resolved by the CLSM, including the effects of topography on incoming solar radiation and on air temperatures, may explain the remaining discrepancies between the SSS simulation and observations.

DISCUSSION

Earlier (A method for partioning the KRB section), we obtained the shallow and deep snowcover fractions by analysing the slope of the snow areal depletion curve over the KRB during May and June of 2002. On the time series of snowcover fraction, a tangent was drawn at the point where the slope of the snow areal depletion curve achieved its greatest absolute value (see Figure 7). The rapid decline in snowcover fraction at this stage of the snowmelt is indicative of a shallow snowpack that ablates quickly and uniformly across the KRB. A second tangent was established at the point where the slope of the snow areal depletion curve attained the specified threshold absolute value of 1% per day. As snowmelt wanes, the slope of the snow areal depletion curve begins to level off as the snowcover fraction attains a secondary plateau. This is indicative of snowdrifts that linger several weeks as they slowly ablate, even though the shallow snowcover fraction has already vanished (Déry *et al.*, 2004). The approximate time at which the shallow snowpack has completely melted is deduced from the intersection of the two tangents. On this date, the shallow and deep snowcover fractions are then inferred from the snow areal depletion curve.

The strategy employed to obtain the shallow and deep snowcover fractions can easily be automated and generalized to multiple watersheds subject to seasonal snowcovers. Time series of the snowcover fraction and its time rate of change are the two necessary inputs required to infer the shallow and deep snowcover areas. Figure 10 illustrates two idealized snow areal depletion curves representing snowmelt over an arbitrary catchment during May. For curve 1, the snow areal depletion curve ends with a secondary plateau near zero, whereas curve 2 achieves a secondary plateau near a snowcover fraction of 20%. Following the procedure outlined before, tangents are drawn along the curves at points where the slope is maximized (in absolute terms) and where it begins to level off again. For curve 1, the intersection of the two tangents provides a deep snowpack covering 10% of the watershed, whereas for curve 2 this fraction increases to 27%.

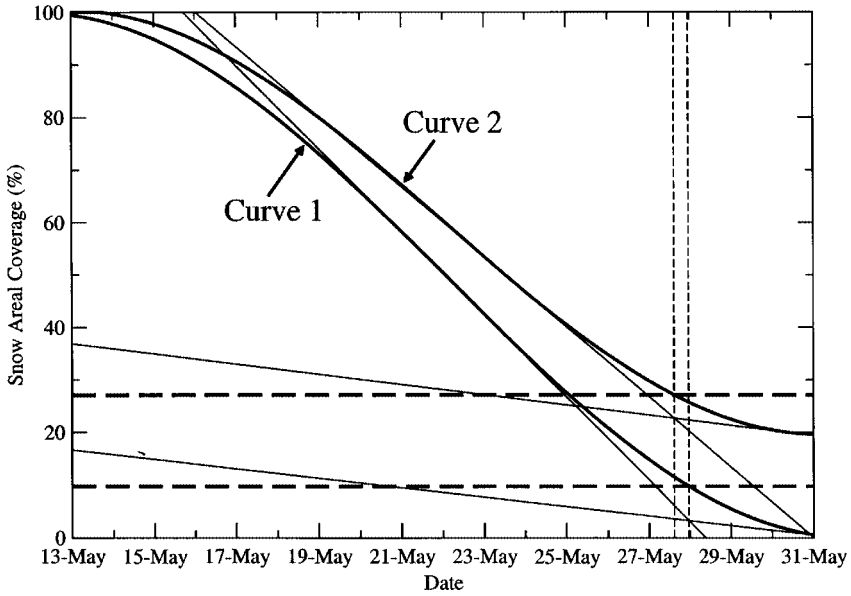

Figure 10. The temporal evolution of snow areal coverage inferred from MODIS for two idealized cases. The characteristics and physical interpretation of curves 1 and 2 are described in the text

From this discussion, we suggest that the shape of a snow areal depletion curve expresses the degree of nonuniformity in the snowpack prior to the ablation period. Curve 1 is representative of a spatially uniform snowpack that melts rapidly and evenly across a watershed, with minimal persistent snow. On the other hand, curve 2 depicts a basin with considerable snow heterogeneity, with a shallow snowpack that melts at about the same rate as curve 1 and a deep snowpack that is much more persistent owing to the large amount of SWE it contains. The information contained in the snow areal depletion curves derived from MODIS can, therefore, be easily extracted and applied to various watersheds.

Despite its simplicity, this automated approach has some limitations. In high-latitude watersheds such as the KRB, frequent episodes of low-level clouds may inhibit MODIS from detecting snow at the surface. This may reduce the temporal resolution of the MODIS snowcover data and degrade the accuracy of the snow areal depletion curves. Late-season snowfalls may complicate the situation by rapidly increasing the snowcover fraction for a few days (Hall and Martinec, 1985). Sudden spikes in the snowcover fraction will need to be filtered out to avoid the negative impact of these precipitation events on the analysis of the deep and shallow snowcover fractions. Special consideration of vegetation and snow masking will also be necessary, since this poses an additional challenge in applying the proposed methodology globally.

SUMMARY AND FUTURE WORK

We have demonstrated that subpixel (<500 m) values of snowcover fraction deduced from MODIS compared favourably with Landsat data. A mean absolute error in snowcover area of 0·07 and a coefficient of determination of 0·90 revealed the high level of accuracy achieved by the MODIS subpixel scheme applied to the North Slope of Alaska. The most prominent discrepancies between MODIS and Landsat measurements were found to occur at fractional values of <0·2. After a correction was applied to remove this bias, the MODIS data can be used to estimate snowcover area at all stages of the snowmelt period in the KRB of Alaska. Bias-corrected snow areal depletion curves for the spring of 2002 exhibited similar features to those inferred from snow-course measurements. A secondary plateau in snowcover area late during the melt period

was associated with the presence of persistent snowdrifts on the arctic landscape. It was found that about 76% of the KRB was covered by a shallow snowpack and the remaining 24% by a deep snowpack. Application of these snowcover fractions in the CLSM subgrid-scale snow parameterization enhanced significantly the simulation of snowcover ablation and of freshwater discharge during the spring transition period for 11 years in the KRB.

Although we have demonstrated the feasibility of using MODIS data to constrain new parameters introduced by the CLSM subgrid-scale snow parameterization, this was achieved in a single basin. In other river basins, variations in the local topography, vegetation, and climate will interact to produce different levels of snowcover heterogeneity. As such, the area covered by shallow and deep snowcovers will vary from catchment to catchment in response to the local environment. To that end, a straightforward methodology that automatically extracts the shallow and deep snowcover fractions based on the evolution of the snow areal depletion curves inferred from MODIS will be applied in all watersheds subject to seasonal snowcovers. These fractions will then be used to provide the necessary parameters for the CLSM subgrid-scale snow parameterization. It is anticipated that incorporation of the MODIS data in the updated CLSM will improve simulations and predictions of the global surface energy and water budgets.

ACKNOWLEDGEMENTS

We acknowledge that funding for M. Steiglitz is provided from National Science Foundation (NSF) grants from the Office of Polar Programs (OPP-002369), from the division of Environmental Biology (Arctic LTER Project), and from an NSF Cooperative Agreement (OPP-0002239), as well as the National Aeronautics and Space Administrations (NASA's) Seasonal-to-Interannual Prediction Project at Goddard Space Flight Center, NASA's Global Modeling and Analysis Program under RTOP 622-24-47, and the NSF Biocomplexity award ATM 0221835. J. Hobbie, G. R. Shaver, and J. M. Laundre (MBL, Woods Hole) are thanked for permitting access to the Arctic LTER database. We express our gratitude to D. L. Kane and L. D. Hinzman (University of Alaska, Fairbanks) for access to snow-course data collected at Imnavait Creek. Comments by R. D. Koster (NASA GSFC) and logistical support from G. A. Riggs and J. Chien (NASA GSFC) and Å. K. Rennermalm (Princeton University) are gratefully acknowledged. E. Gómez-Landesa (New Mexico State University) and an anonymous reviewer provided helpful comments on the manuscript. This work is Lamont–Doherty Earth Observatory contribution #6621.

REFERENCES

Ackerman SA, Strabala KI, Menzel PWP, Frey RA, Moeller CC, Gumley LE. 1998. Discriminating clear sky from clouds with MODIS. *Journal of Geophysical Research* **103**: 32 141–32 157.

Andreas EL. 1995. Air–ice drag coefficients in the western Weddell Sea, 2. A model based on form drag and drifting snow. *Journal of Geophysical Research* **100**(C3): 4833–4843.

Arola A, Lettenmaier DP. 1996. Effects of subgrid spatial heterogeneity on GCM-scale land surface energy and moisture fluxes. *Journal of Climate* **9**: 1339–1349.

Barnes WL, Pagano TS, Salomonson VV. 1998. Prelaunch characteristics on the moderate resolution imaging spectroradiometer (MODIS) on EOS-AM1. *IEEE Transactions on Geoscience and Remote Sensing* **36**: 1088–1100.

Bowling LC, Kane DL, Gieck RE, Hinzman LD, Lettenmaier DP. 2003. The role of surface storage in a low-gradient arctic watershed. *Water Resources Research* **39**(4): 1087. DOI: 10·1029/2002WR001466.

Brown RD, Braaten RO. 1998. Spatial and temporal variability of Canadian monthly snow depths. *Atmosphere–Ocean* **36**: 37–54.

Chapman WL, Walsh JE. 1993. Recent variations in sea ice and air temperature in high latitudes. *Bulletin of the American Meteorological Society* **74**: 33–47.

Crane RG, Anderson MR. 1984. Satellite discrimination of snow/cloud surface. *International Journal of Remote Sensing* **5**(1): 213–223.

Curtis J, Wendler G, Stone R, Dutton E. 1998. Precipitation decrease in the western Arctic, with special emphasis on Barrow and Barter Island, Alaska. *International Journal of Climatology* **18**: 1687–1707.

Déry SJ, Taylor PA. 1996. Some aspects of the interaction of blowing snow with the atmospheric boundary layer. *Hydrological Processes* **10**: 1345–1358.

Déry SJ, Yau MK. 1999. A climatology of adverse winter-type weather events. *Journal of Geophysical Research* **104**: 16 657–16 672.

Déry SJ, Yau MK. 2001a. Simulation of an Arctic ground blizzard using a coupled blowing snow–atmosphere model. *Journal of Hydrometeorology* **2**: 579–598.
Déry SJ, Yau MK. 2001b. Simulation of blowing snow in the Canadian Arctic using a double-moment model. *Boundary-Layer Meteorology* **99**: 297–316.
Déry SJ, Yau MK. 2002. Large-scale mass balance effects of blowing snow and surface sublimation. *Journal of Geophysical Research* **107**: 4679. DOI: 10·1029/2001JD001251.
Déry SJ, Taylor PA, Xiao J. 1998. The thermodynamic effects of sublimating, blowing snow in the atmospheric boundary layer. *Boundary-Layer Meteorology* **89**: 251–283.
Déry SJ, Crow WT, Stieglitz M, Wood EF. 2004. Modeling snow-cover heterogeneity over complex arctic terrain for regional and global climate models. *Journal of Hydrometeorology* **5**: 33–48.
Dozier J. 1989. Spectral signature of alpine snow cover from the Landsat thematic mapper. *Remote Sensing of Environment* **28**: 9–22.
Ducharne A, Koster RD, Suarez MJ, Stieglitz M, Kumar P. 2000. A catchment-based approach to modeling land surface processes in a general circulation model, 2. Parameter estimation and model demonstration. *Journal of Geophysical Research* **105**: 24 823–24 838.
Ellis AW, Leathers DJ. 1998. The effects of a discontinuous snow cover on lower atmospheric temperature and energy flux patterns. *Geophysical Research Letters* **25**: 2161–2164.
Foster JL. 1989. The significance of the date of snow disappearance on the arctic tundra as a possible indicator of climate change. *Arctic and Alpine Research* **21**: 60–70.
Hall DK. 1988. Assessment of polar climate change using satellite technology. *Reviews of Geophysics* **26**: 26–39.
Hall DK, Martinec J. 1985. *Remote Sensing of Ice and Snow*. Chapman and Hall.
Hall DK, Riggs GA, Salomonson VV. 1995. Development of methods for mapping global snow cover using moderate resolution imaging spectroradiometer (MODIS) data. *Remote Sensing of Environment* **54**: 127–140.
Hall DK, Riggs GA, Salomonson VV, DiGirolamo NE, Bayr KJ. 2002a. MODIS snowcover products. *Remote Sensing of Environment* **83**: 181–194.
Hall DK, Kelly REJ, Riggs GA, Chang ATC, Foster JL. 2002b. Assessment of the relative accuracy of hemispheric-scale snow-cover maps. *Annals of Glaciology* **34**: 24–30.
Holmgren B, Benson C, Weller G. 1975. A study of the breakup on the Arctic Slope of Alaska by ground, air and satellite observations. In *Climate of the Arctic*, Weller G, Bowling S (eds). Geophysical Institute, University of Alaska: Fairbanks; 348–356.
Kane DL, Hinzman LD. 2003. *Meteorological and hydrographic data, Kuparuk River watershed*. National Snow and Ice Data Center, digital media. http://nsidc.org/data/arcss015.html (14 June 2003).
Kane DL, Hinzman LD, McNamara JP, Zhang Z, Benson CS. 2000. An overview of a nested watershed study in arctic Alaska. *Nordic Hydrology* **31**: 245–266.
Kaufman YJ, Kleidman RG, Hall DK, Martins JV, Barton JS. 2002. Remote sensing of subpixel snow cover using 0·66 and 2·1 μm channels. *Geophysical Research Letters* **29**(16): DOI: 10·1029/2001GL013580.
Klein AG, Barnett AC. 2003. Validation of daily MODIS snow cover maps of the Upper Rio Grande river basin for the 2000–01 snow year. *Remote Sensing of Environment* **86**: 162–176.
Klein AG, Hall DK, Riggs GA. 1998. Improving snow cover mapping in forests through the use of a canopy reflectance model. *Hydrological Processes* **12**: 1723–1744.
König M, Sturm M. 1998. Mapping snow distribution in the Alaskan Arctic using aerial photography and topographic relationships. *Water Resources Research* **34**: 3471–3483.
Koster RD, Suarez MJ, Ducharne A, Stieglitz M, Kumar P. 2000. A catchment-based approach to modeling land surface processes in a general circulation model, 1. Model structure. *Journal of Geophysical Research* **105**: 24 809–24 822.
Li S, Sturm M. 2002. Patterns of wind-drifted snow on the Alaska arctic slope detected with ERS-1 interferometric SAR. *Journal of Glaciology* **48**(163): 495–504.
Liston GE. 1995. Local advection of momentum, heat, and moisture during the melt of patchy snow covers. *Journal of Applied Meteorology* **34**: 1705–1715.
Liston GE. 1999. Interrelationships among snow distribution, snowmelt, and snow cover depletion: implications for atmospheric, hydrologic, and ecologic modeling. *Journal of Applied Meteorology* **38**: 1474–1487.
Luce CH, Tarboton DG, Cooley KR. 1998. The influence of the spatial distribution of snow on basin-averaged snowmelt. *Hydrological Processes* **12**: 1671–1683.
Lynch AH, McGinnis DL, Bailey DA. 1998. Snow–albedo feedback and the spring transition in a regional climate system model: influence of land surface model. *Journal of Geophysical Research* **103**: 29 037–29 049.
Lynch-Stieglitz M. 1994. The development and validation of a simple snow model for the GISS GCM. *Journal of Climate* **7**(12): 1842–1855.
Maurer EP, Rhoads JD, Dubayah RO, Lettenmaier DP. 2003. Evaluation of the snow-covered area data product from MODIS. *Hydrological Processes* **17**: 59–71.
McNamara JP, Kane DL, Hinzman LD. 1998. An analysis of streamflow hydrology in the Kuparuk River basin, arctic Alaska: a nested watershed approach. *Journal of Hydrology* **206**: 39–57.
Myneni RB, Keeling CD, Tucker CJ, Asrar G, Nemani RR. 1997. Increased plant growth in the northern high latitudes from 1981 to 1991. *Nature* **386**: 698–702.
Peterson BJ, Holmes RM, McClelland JW, Vörösmarty CJ, Lammers RB, Shiklomanov AI, Shiklomanov IA, Rahmstorf S. 2002. Increasing river discharge to the Arctic Ocean. *Science* **298**: 2171–2173.
Pomeroy JW, Gray DM. 1995. *Snowcover accumulation, relocation and management*. NHRI Science Report 7, Saskatoon, SK, USA.
Ramsay BH. 1998. The interactive multisensor snow and ice mapping system. *Hydrological Processes* **12**: 1537–1546.
Salomonson VV, Appel I. 2004. Estimating fractional snow cover from MODIS using the normalized difference snow index (NDSI). *Remote Sensing of Environment* **89**: 351–360.
Serreze MC, Lynch AH, Clark MP. 2001. The arctic frontal zone as seen in the NCEP–NCAR reanalysis. *Journal of Climate* **14**: 1550–1567.

Shaman J, Stieglitz M, Engel V, Koster R, Stark C. 2002. Representation of subsurface storm flow and a more responsive water table in a TOPMODEL-based hydrology model. *Water Resources Research* **38**(8): 1156. DOI: 10·1029/2001WR000636.

Sheffield J, Pan M, Wood EF, Mitchell KE, Houser PR, Schaake JC, Robock A, Lohmann D, Cosgrove B, Duan Q, Luo L, Higgins RW, Pinker RT, Tarpley JD, Ramsay BH. 2003. Snow process modeling in the North American Land Data Assimilation System (NLDAS): 1. Evaluation of model-simulated snow cover extent. *Journal of Geophysical Research* **108**(D22): 8849. DOI: 10·1029/2002JD003274.

Sorooshian S, Whitaker MPL, Hogue TS. 2002. Regional and global hydrology and water resources issues: the role of international and national programs. *Aquatic Sciences* **64**: 317–327.

Stieglitz M, Hobbie J, Giblin A, Kling G. 1999. Hydrologic modeling of an arctic tundra watershed: toward pan-Arctic predictions. *Journal of Geophysical Research* **104**: 27 507–27 518.

Stieglitz M, Ducharne A, Koster R, Suarez M. 2001. The impact of detailed snow physics on the simulation of snow cover and subsurface thermodynamics at continental scales. *Journal of Hydrometeorology* **2**: 228–242.

Stieglitz M, Déry SJ, Romanovsky VE, Osterkamp TE. 2003. The role of snow cover in the warming of arctic permafrost. *Geophysical Research Letters* **30**(13): 1721. DOI: 10·1029/2003GL017337.

Sturm M, Liston GE, Benson CS, Holmgren J. 2001. Characteristics and growth of a snowdrift in arctic Alaska, U.S.A. *Arctic, Antarctic and Alpine Research* **33**: 319–329.

Vaganov EA, Hughes MK, Kirdyanov AV, Schweingruber FH, Silkin PP. 1999. Influence of snowfall and melt timing on tree growth in subarctic Eurasia. *Nature* **400**: 149–151.

Vikhamer D, Solberg R. 2002. Subpixel mapping of snow cover in forests by optical remote sensing. *Remote Sensing of Environment* **83**: 97–111.

Woo MK. 1986. Permafrost hydrology in North America. *Atmosphere–Ocean* **24**(3): 201–234.

Ye H, Cho HR, Gustafson PE. 1998. The changes in Russian winter snow accumulation during 1936–83 and its spatial patterns. *Journal of Climate* **11**: 856–863.

Zhang T, Stamnes K, Bowling SA. 1996. Impact of clouds on surface radiative fluxes and snowmelt in the Arctic and Subarctic. *Journal of Climate* **9**: 2110–2123.

Zhang T, Stamnes K, Bowling SA. 2001. Impact of the atmospheric thickness on the atmospheric downwelling longwave radiation and snowmelt under clear-sky conditions in the Arctic and Subarctic. *Journal of Climate* **14**: 920–939.

